Deciphering the role of the electrostatic interactions in the α-tropomyosin head-to-tail complex

Fernando Corrêa,[1] Roberto Kopke Salinas,[1*] Alexandre M. J. J. Bonvin,[2] and Chuck S. Farah[1*]

[1] Departamento de Bioquímica, Instituto de Química, Universidade de São Paulo, São Paulo, SP, Brazil

[2] Bijvoet Center for Biomolecular Research, Science Faculty, Utrecht University, 3584CH, Utrecht, The Netherlands

ABSTRACT

Skeletal α-tropomyosin (Tm) is a dimeric coiled-coil protein that forms linear assemblies under low ionic strength conditions in vitro through head-to-tail interactions. A previously published NMR structure of the Tm head-to-tail complex revealed that it is formed by the insertion of the N-terminal coiled-coil of one molecule into a cleft formed by the separation of the helices at the C-terminus of a second molecule. To evaluate the contribution of charged residues to complex stability, we employed single and double-mutant Tm fragments in which specific charged residues were changed to alanine in head-to-tail binding assays, and the effects of the mutations were analyzed by thermodynamic double-mutant cycles and protein–protein docking. The results show that residues K5, K7, and D280 are essential to the stability of the complex. Though D2, K6, D275, and H276 are exposed to the solvent and do not participate in intermolecular contacts in the NMR structure, they may contribute to head-to-tail complex stability by modulating the stability of the helices at the Tm termini.

Key words: tropomyosin; coiled-coil; double-mutant thermodynamic cycles; muscle; protein–protein docking.

INTRODUCTION

Skeletal muscle α-tropomyosin (Tm) is an α-helical protein composed of 284 residues, which adopts an in-register coiled-coil conformation. It forms linear polymers due to a head-to-tail association of its N- and C-termini, and this polymer lies along the long pitch strands of the F-actin filament.[1–4] McLachlan and Stewart[3] observed that the overlapping of the Tm ends reduces its effective length to 275 aminoacids (410 Å), which is close to the observed value of Tm length repeat in crystals.[3,5] This overlap would allow the Tm periodicity to continue unbroken from one molecule to the next, in register with actin in the thin filament. There is a large body of experimental evidence indicating that electrostatic interactions play an important role in Tm polymerization: acetylation of residue K7 abolished Tm polymerization,[6] and phosphorylation of S283[7,8] and its mutation to Glu increased Tm viscosity.[9] Furthermore, Tm polymerization *in vitro* is strongly dependent on ionic strength.[10–13] In the first molecular model, proposed for the head-to-tail interaction by McLachlan and Stewart,[3] the complex was formed by an external overlap of the flat broad faces of the supercoil at the N- and C-termini. This model proposed the existence of intermolecular electrostatic interactions between positively charged N-terminal residues and negatively charged C-terminal residues.

Recently, a solution NMR structure of the head-to-tail complex (Tm1a$_{1–14}$Zip–Tm9a$_{251–284}$) was solved.[14] Surprisingly, the structure showed a symmetric interleaved packing interaction in which the helical chains of the C-terminal region spread apart to allow the insertion of the N-terminal coiled-coil into the resulting cleft. This complex is stabilized mainly by hydrophobic interactions involving N-terminal residues M1, I4, M8, and L11, and C-terminal residues L274, A277, M281, and I284. Most of the electrostatic interactions were intrachain and only a few intermolecular electrostatic interactions were observed (K5–D280, K5–E273 and for the K5, K7, and K12 side-chains with the C-terminal COO$^-$ group of I284) leading to the proposal that ionic interactions could be contributing mainly to the stability of the individual helical chains.[14]

To extend our understanding of the role of electrostatic interactions on the stability of the head-to-tail complex, we have undertaken a study of the contribution

of specific charged residues (D2, K5, K6, K7, D275, H276, and D280) on complex formation. The effects of single and double-mutants on the association equilibrium were used to construct double-mutant thermodynamic cycles[15–19] to identify the energetics of possible intermolecular salt bridges. This data was also used to drive the docking of wild-type and mutated fragments to produce molecular models of the mutant complexes. We observed that the K5A, K7A, and D280A mutations drastically affected the head-to-tail interaction, consistent with their participation in salt bridges in the NMR structure.[14] Interestingly, the D275A mutation also reduced complex stability even though this residue is completely exposed to the solvent in the solution structure.[14] The results described here provide insights into the structural and energetic contributions of the charged residues to head-to-tail complex formation.

METHODS

Construction of expression vectors, expression, and purification of Tm fragments

The plasmid vectors and bacterial expression of the $ASTm_{1–142}$ fragment (residues 1–142 of chicken skeletal α-Tm with an Ala–Ser N-terminal fusion) and $Tm_{143–284(5OHW269)}$ fragment (residues 143–284 of chicken skeletal α-Tm with a 5-hydroxytryptophan residue at position 269) have been described previously.[13,20–23] Single site-directed mutagenesis of residues D2, K5, K6, K7, D275, H276, and D280 were performed in a single-step PCR using the QuickChange Site-Directed Mutagenesis kit (STRATAGENE). The oligonucleotides used to mutate the residues are listed in Table I. The $ASTm_{1–142}$ fragment and its mutants were purified as described in Refs. 20 and 22, while the $Tm_{143–284(5OHW269)}$ fragment and its mutants were purified as described in Refs. 13 and 21. Protein concentrations were determined by the modified Lowry method.[24]

Fluorescence titrations and determination of head-to-tail complex dissociation constants

Titration assays were performed using an AVIV (Lakewood, NJ) ATF105 automated titration differential/ratio spectrofluorometer. The 5-hydroxytryptophan emission fluorescence spectra of $Tm_{143–284(5OHW269)}$ and C-terminal mutants (2 μM) were collected between 338 and 342 nm (bandwidth: 5–7 nm) using an excitation wavelength of 295 nm (bandwidth: 0.5–1 nm). Fluorescence emission spectra were collected after addition of aliquots of $ASTm_{1–142}$ or N-terminal mutants in 0.2 μM (dimer) increments. The samples were equilibrated for 3 min before each measurement. The proteins were dissolved in 54.5 mM MOPS (3-(N-morpholino)propanesulfonic acid) pH 7.0, 0.5 mM EDTA, 1 mM 1,4 dithiothreitol

Table I

List of Oligonucleotides Used for Site-Directed Mutagenesis of Tm Fragments

Mutant	Oligonucleotide sequence
D2A	5′-TAT GGC TAG CAT G**GC T**GC CAT CAA GAA AAA GAT-3′
D2A[a]	5′-CAT CTT TTT CTT GAT GGC **AGC** CAT GCT AGC CAT A-3′
K5A	5′-GCT AGC ATG GAT GCC ATC **GCG** AAA AAG ATG CAG ATG CTG AAA-3′
K5A[a]	5′-TTT CAG CAT CTG CAT CTT TTT **CGC** GAT GGC ATC CAT GCT AGC-3′
K6A	5′-GCA TGG ATG CCA TCA AG**G CA**A AGA TGC AGA TGC TG-3′
K6A[a]	5′-CAG CAT CTG CAT CTT **TGC** CTT GAT GGC ATC CAT GC-3′
K7A	5′-AGC ATG GAT GCC ATC AAG AAA **GCG** ATG CAG ATG CTG AAA CTG-3′
K7A[a]	5′-CAG TTT CAG CAT CTG CAT **CGC** TTT CTT GAT GGC ATC CAT GCT-3′
D275A	5′-ATC AGC GAG GAG CTG **GCC** CAT GCT CTC AAC GAT-3′
D275A[a]	5′-ATC GTT GAG AGC ATG **GGC** CAG CTC CTC GCT GAT-3′
H276A	5′-GCG AGG AGC TGG AC**G CT**G CTC TCA ACG ATA TG-3′
H276A[a]	5′-CAT ATC GTT GAG AGC **AGC** GTC CAG CTC CTC GC-3′
H276E	5′-ATC AGC GAG GAG CTG GAC **GAG** GCT CTC AAC GAT ATG ACT TCC-3′
H276E[a]	5′-GGA AGT CAT ATC GTT GAG AGC **CTC** GTC CAG CTC CTC GCT GAT-3′
D280A	5′-TGG ACC ATG CTC TCA AC**G CT**A TGA CTT CCA TAT AA-3′
D280A[a]	5′-TTA TAT GGA AGT CAT **AGC** GTT GAG AGC ATG GTC CA-3′

The mutated codon is in bold type and mutated nucleotides are underlined.
[a]Antisense oligonucleotide.

(DTT) or 25 mM MOPS pH 7.0, 5 mM MgCl$_2$, 1 mM DTT at 25°C. Dissociation constants were determined using a nonlinear regression fitting of fluorescence titration curves to Eq. (1).[23]

$$F = (\nu/V)((\alpha - 1)/(2[C]_{\text{total}})([N]_{\text{total}} + [C]_{\text{total}} + K_d$$
$$- (((([N]_{\text{total}} + [C]_{\text{total}} + K_d)^2) - 4[N]_{\text{total}}[C]_{\text{total}})^{1/2}) + 1) \quad (1)$$

where F is the fluorescence intensity at any given point in the titration curve, ν is the initial volume, V is volume at any given point in the titration, $[N]_{\text{total}}$ and $[C]_{\text{total}}$ are the total N- or C-terminal fragment concentrations at any given point in the titration curve, K_d is the dissociation constant, and α is the ratio between the maximum fluorescence intensity of the head-to-tail complex and that of the free C-terminal fragment (initial fluorescence intensity).

Standard free energies of dissociation (ΔG_{NC}) were calculated from dissociation constants. The free energy of coupling (ΔG_i) for each interaction pair was calculated as follows:

$$\Delta G_i = (\Delta G_{\text{NC}} - \Delta G_{\text{N}\underline{\text{C}}}) - (\Delta G_{\underline{\text{N}}\text{C}} - \Delta G_{\underline{\text{N}}\underline{\text{C}}})$$
$$= (\Delta G_{\text{NC}} - \Delta G_{\text{N}\underline{\text{C}}}) - (\Delta G_{\underline{\text{N}}\text{C}} - \Delta G_{\underline{\text{N}}\underline{\text{C}}}) \quad (2)$$

where $\Delta G_{\text{N}\underline{\text{C}}}$ and $\Delta G_{\underline{\text{N}}\text{C}}$ are standard free energies of single-mutant interactions of C-terminal and N-terminal mutants, respectively. $\Delta G_{\underline{\text{N}}\underline{\text{C}}}$ is the standard free energy of dissociation for a double-mutant.[15–19]

The standard deviations in ΔG_i were calculated using Eq. (3), as described in Ref. 25:

$$\sigma_{\Delta G_i} = [(\sigma \Delta G_{NC})^2 + (\sigma \Delta G_{\underline{N}C})^2 + (\sigma \Delta G_{N\underline{C}})^2 + (\sigma \Delta G_{\underline{NC}})^2]^{1/2} \quad (3)$$

The $\sigma_{\Delta G_i}$ for the experiments were on average 0.32 kcal/mol. Therefore, when ΔG_i is in the range of ± 0.32 kcal/mol, the effects of mutating those two residues in the head-to-tail interface are considered additive.

Thermal denaturation monitored by circular dichroism

The conformational stability of Tm fragments were analyzed by thermal denaturations followed by measuring the negative ellipticity at 222 nm. The measurements were collected at 2°C intervals from 4 to 80°C and back to 4°C at a velocity of 1°C/min. The proteins were dissolved (10 μM dimer) in 54.5 mM MOPS pH 7.0, 0.5 mM EDTA, 1 mM DTT or 25 mM MOPS pH 7.0, 5 mM MgCl₂, 1 mM DTT at 25°C.

Protein–protein docking

The coordinates of models for the free N-terminal and C-terminal fragments were built from the published NMR structure of the Tm head-to-tail complex[14] (PDB 2G9J—Model 1). The C-terminal peptide (Tm$_{268-284}$269W) was built from residues 268–284 of the NMR structure with changes at two residues: A269W and K279N. The N-terminal peptide (ASTm$_{1-15}$) was built from the coordinates of residues 1–15 to which an Ala–Ser N-terminal fusion dipeptide was added—residues A(−1) and S(0). In this way, both peptide sequences are similar to the ones used in our binding experiments; the only difference being that tryptophan instead of 5-hydroxytryptophan was modeled at position 269. These two starting ("wild-type") structures, as well as the other mutant structures (D2A, K6A, K7A, D275A, H276A, H276E, D2A–D275A, D2A–H276A, D2A–H276E, K6A–H276A, K6A–H276E, K7A–H276A, and K7A–H276E) were built by homology modeling using MODELLER[26] from the InsightII-2000 package (Accelrys).
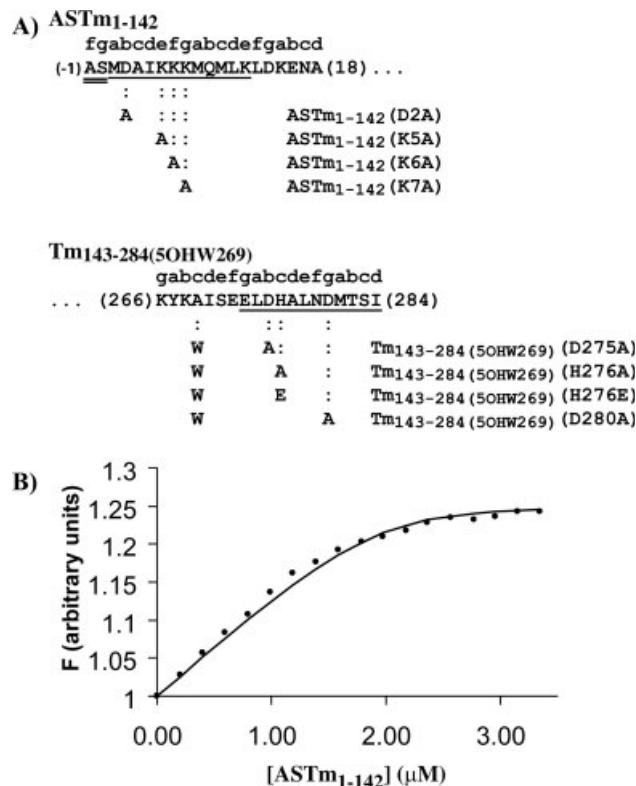
The protein–protein docking calculations were performed with HADDOCK1.3 using CNS1.1[27,28] with the parallhdg5.3 force field and the OPLSX nonbonded parameters.[29] The docking was driven by ambiguous interaction restraints (AIRs), which are defined as ambiguous distance restraints of the active residues of one protein interface with the selected active and passive residues of the other protein interface.[28,30] Residues that were identified to be important for binding according to our mutagenesis data were defined as active: for the C-terminal interface, D280 was active while the neighboring residues

A277, M281, S283, and I284 were considered passives; for the N-terminal, K5 was active while the neighboring residues I4 and K7 were considered passives. A more specific AIR was also introduced between L278 and A3, since an interaction was observed in the NMR structure,[14] and mutation of one or other to Cys abolishes the interaction (data not shown). This additional restraint allowed a better fitting of the N-terminal into C-terminal cleft in the docking of the unmutated fragments. For the docking of the mutants, we have assumed that all AIRSs, which do not involve the mutated residue, were preserved. The segments comprising residues −1 to 14 and 273 to 284 were considered as interface and treated as semiflexible during the docking, while the remaining residues were kept rigid. In addition, we imposed standard helical dihedral angle restraints (psi = 40° ± 10, phi = −60° ± 10), hydrogen bonding restraints, and two helix–helix distance restraints to keep the two chains parallel in the case of the C-terminal, and to maintain the coiled-coil in case of the N-terminal. For the C-terminus, the helix–helix restraints[31] were defined such that the interchain distances between Cα atoms of residues 268, 269, and 270 were kept at a distance similar to that observed in the NMR structure.[14] These residues lie outside the overlap region in which the strands were free to separate. Similar restraints were used for residues 8–10 in the N-terminus. C2 symmetry restraints[32] were used to maintain the symmetry of the complex. The docking protocol consisted of an initial rigid body energy minimization (1000 models) in which rotational and translational movements were allowed and the AIR energy term was minimized. The structures were sorted according to the Haddock score ($0.1 \times E_{vdw} + E_{elec} + E_{AIR} + E_{sym} - 0.01 \times E_{BSA}$) and the top 200 structures were submitted to a semiflexible simulated annealing in torsion angle space followed by refinement in explicit solvent (water) (for details of the protocol, see Ref. 28). The final structures were sorted according to the Haddock score ($E_{vdw} + 0.2 \times E_{elec} + E_{AIR} + 0.1 \times E_{sym}$) and clustered using a 1.5 Å RMSD cutoff. Clusters with the lowest average intermolecular energies were analyzed for intermolecular contacts (hydrogen bonds, van der Waals) using LIGPLOT.[33] The backbone RMSD was calculated using atoms N, Cα, and C' from residues 1–14 from the N-terminus, and residues 268–280 from the C-terminus, using PROFIT (A.C.R. Martin, www.bioinf.org.uk/software/profit).

RESULTS

Effect of single and double mutations on tropomyosin head-to-tail complex formation

An inspection of the primary structure of the Tm N-terminal fragment shows that it is rich in positively charged residues (MDAI**KKK**MQML**K**L), while the

A) ASTm$_{1-142}$

```
        fgabcdefgabcdefgabcd
(-1) ASMDAIKKKMQMLKLDKENA(18)...
       :   :::
     A :::              ASTm1-142 (D2A)
        A::             ASTm1-142 (K5A)
         A:             ASTm1-142 (K6A)
          A             ASTm1-142 (K7A)
```

Tm$_{143-284(5OHW269)}$

```
         gabcdefgabcdefgabcd
... (266) KYKAISEELDHALNDMTSI(284)
             :    ::    :
             W    A:    :   Tm143-284 (5OHW269) (D275A)
             W    A     :   Tm143-284 (5OHW269) (H276A)
             W    E     :   Tm143-284 (5OHW269) (H276E)
             W          A   Tm143-284 (5OHW269) (D280A)
```

B)

Figure 1

(**A**) Sequences at the termini of mutant fragments. The first twenty residues of ASTm$_{1-142}$ and the last nineteen residues of Tm$_{143-284(5OHW269)}$ are shown. Heptad repeat positions are shown above the sequences. Mutated residues are indicated below each sequence for each corresponding fragment. Amino acids involved in the formation of the head-to-tail complex in native Tm are underlined. The Ala–Ser N-terminal extension in ASTm$_{1-142}$ is double underlined. (**B**) Titration of Tm$_{143-284(5OHW269)}$ with ASTm$_{1-142}$, as monitored by fluorescence. Tm$_{143-284(5OHW269)}$ (2 μM) was titrated with 0.2 μM increments of ASTm$_{1-142}$. The data were fitted to Eq. (1) (Methods section) to calculate the K_d for the formation of head-to-tail complex. The same experiment was repeated with all possible combinations of mutant fragments from the N-terminal and C-terminal in two buffer conditions: 54.5 mM MOPS pH 7.0, 0.5 mM EDTA, 1 mM DTT or 25 mM MOPS pH 7.0, 5 mM MgCl$_2$ and 1 mM DTT at 25°C. Calculated K_d values are listed in Table II.

C-terminal region is rich in negatively charged residues (S**E**E**L**DHAL**N**DMTSI). To evaluate the contributions of each charged residue from the head-to-tail interface to the stability of the complex, we built a series of Tm recombinant fragments containing single amino acid substitutions in the N-terminus [ASTm$_{1-142}$, ASTm$_{1-142}$(D2A), ASTm$_{1-142}$(K5A), ASTm$_{1-142}$(K6A), and ASTm$_{1-142}$(K7A)] and the C-terminus [Tm$_{143-284(5OHW269)}$, Tm$_{143-284(5OHW269)}$(D275A), Tm$_{143-284(5OHW269)}$(D280A), Tm$_{143-284(5OHW269)}$(H276A), and Tm$_{143-284(5OHW269)}$(H276E)]. [Fig. 1(A)] The N-terminal fragments have an Ala–Ser N-terminal extension necessary for polymerization of recombinant Tm produced in bacteria.[20] The C-terminal fragments contained a 5-hydroxytryptophan (5OHW) probe at position 269, which is located 15 resi-

dues away from the C-terminus of the polypeptide chain. The fluorescence of this tryptophan analog has been shown to be a sensitive probe of the polymerization state of Tm.[13,22,23,34] The use of fragments rather than full-length Tm is advantageous, because it reduces the complex polymerization process[13] to a simple dimerization, allowing a more facile determination of the dissociation constant and energy of association involved in complex formation.[23]

Titrations of all possible combinations of N- and C-terminal fragments were performed by following the changes in the fluorescence emission of the 5OHW-labelled C-terminal fragment upon addition of N-terminal fragments [Fig. 1(B) and data not shown]. The titration curves were then used to calculate dissociation constants of the complexes (Table II) as described in Methods section. The binding assays were performed both in the absence and in the presence of 5 mM MgCl$_2$, to evaluate the influence of Mg^{2+} on complex formation.

Table II shows that, in the absence of Mg^{2+}, substitution of K5 or K7 in the N-terminal, or D280 in the C-terminal for Ala, reduces the affinity to levels below the sensitivity of the fluorescence assay (K_d as high as 2 × 10^{-5} M can be detected). Mutations of K6A and D275A also decrease the affinity from 4.4 ± 1.5 × 10^{-7} M observed for the wild-type complex to 1.5 ± 0.6 × 10^{-6} M and 1.7 ± 0.9 × 10^{-5} M, respectively. On the other hand, the H276A mutation increased the affinity (~10 times) and also could strengthen the interaction that was diminished by the K6A and K7A mutations (K5A–H276A, K7A–H276A). Interestingly, the H276E mutation also resulted in a slight increase in affinity on its own (1.1 ± 0.6 × 10^{-7} M), and could restore the interaction that was lost by the K5A and K7A mutations (K5A–H276E, K7A–H276E). Similarly, the D2A mutant presented a slightly increased affinity on its own (1.7 ± 0.8 × 10^{-7} M) and restored the interaction reduced by the D275A mutation (5.9 ± 2.0 × 10^{-6} M) or lost by D280A (1.1 ± 0.8 × 10^{-6} M).

Addition of Mg^{2+} did not significantly affect the stability of the wild-type complex, but had different effects on the binding affinity of the mutated fragments. Some interactions involving mutants K7A (K7A–H276E, K7A–H276A) and D275A (D275A and D2A–D275A) were reduced to below the detection limit, and in the case of H276A, reduced by an order of magnitude. On the other hand, Mg^{2+} restored formation of some mutant complexes (D280A, 5.6 ± 1.3 × 10^{-6} M; K5A 6.7 ± 1.4 × 10^{-7} M; K5A–H276A, 4.0 ± 1.3 × 10^{-7} M) and increased the binding affinity of others (H276E, ~10 times; D2A–H276E, ~35 times) (Table II).

Double-mutant thermodynamic cycles

The energy of the interaction between two residues can in principle be measured through the combination

Table II
Dissociation Constants and Free Energy of Dissociation for Single and Double Mutant Complexes

ASTm$_{1-142}$	Tm$_{143-284}$ (5OHW269)	K_d ($\times 10^{-7} M$)	ΔG (kcal/mol)	ΔG_i (kcal/mol)	Distance (Å) in PDB 2G9J
Wild-type	Wild-type	(1) 4.4 ($\pm$1.5)	(1) 8.7		
		(2) 2.6 ($\pm$0.9)	(2) 9.0		
D2A	Wild-type	(1) 1.7 ($\pm$0.8)	(1) 9.2		
		(2) 1.1 ($\pm$0.7)	(2) 9.5		
K5A	Wild-type	(1) n.d.	(1) <5.4		
		(2) 6.7 ($\pm$1.5)	(2) 8.4		
K6A	Wild-type	(1) 15.2 ($\pm$0.6)	(1) 7.9		
		(2) 30.4 ($\pm$2.1)	(2) 7.5		
K7A	Wild-type	(1) n.d.	(1) <5.4		
		(2) n.d.	(2) <5.4		
Wild-type	D275A	(1) 173 ($\pm$91.0)	(1) 6.5		
		(2) n.d.	(2) <5.4		
Wild-type	H276A	(1) 0.1 ($\pm$0.5)	(1) 10.6		
		(2) 2.9 ($\pm$2.5)	(2) 8.9		
Wild-type	H276E	(1) 1.1 ($\pm$0.6)	(1) 9.5		
		(2) 0.3 ($\pm$1.5)	(2) 10.1		
Wild-type	D280A	(1) n.d.	(1) <5.4		
		(2) 56.4 ($\pm$13.1)	(2) 7.1		
D2A	D275A	(1) 59.5 ($\pm$20.0)	(1) 7.1	(1) 0.0 ($\pm$0.3)	11.8 ($\pm$2.3)
		(2) n.d.	(2) <5.4	(2) —	OD $\leftrightarrow$ OD
D2A	H276A	(1) 0.28 ($\pm$0.4)	(1) 10.3	(1) $-$0.9 ($\pm$0.3)	17.4 ($\pm$1.4)
		(2) 0.26 ($\pm$1.3)	(2) 10.4	(2) 1.0 ($\pm$0.6)	OD $\leftrightarrow$ ND
D2A	H276E	(1) 2.1 ($\pm$0.0)	(1) 9.1	(1) $-$0.0 ($\pm$0.3)[a]	
		(2) 0.0 ($\pm$0.1)	(2) 11.2	(2) 0.5 ($\pm$0.5)[a]	
D2A	D280A	(1) 10.8 ($\pm$8.0)	(1) 8.1	(1) >2.1 ($\pm$0.3)	12.9 ($\pm$1.8)
		(2) 7.3 ($\pm$2.6)	(2) 8.3	(2) 0.7 ($\pm$0.4)	OD $\leftrightarrow$ OD
K5A	D275A	(1) n.d.	(1) <5.4	(1) —	11.2 ($\pm$0.6)
		(2) n.d.	(2) <5.4	(2) —	NZ $\leftrightarrow$ OD
K5A	H276A	(1) n.d.	(1) <5.4	(1) —	9.6 ($\pm$1.0)
		(2) 4.0 ($\pm$1.3)	(2) 8.7	(2) 0.4 ($\pm$0.4)	NZ $\leftrightarrow$ ND
K5A	H276E	(1) 1.0 ($\pm$0.9)	(1) 9.5	(1) <$-$5.3 ($\pm$0.3)[a]	
		(2) 3.6 ($\pm$1.1)	(2) 8.8	(2) 1.2 ($\pm$0.5)[a]	
K5A	D280A	(1) n.d.	(1) <5.4	(1) —	4.5 ($\pm$1.5)
		(2) n.d.	(2) <5.4	(2) <$-$1.1 ($\pm$0.2)	NZ $\leftrightarrow$ OD
K6A	D275A	(1) n.d.	(1) <5.4	(1) <$-$0.3 ($\pm$0.2)	16.1 ($\pm$2.5)
		(2) n.d.	(2) <5.4	(2) —	NZ $\leftrightarrow$ OD
K6A	H276A	(1) 1.9 ($\pm$1.6)	(1) 9.2	(1) $-$0.7 ($\pm$0.5)	18.1 ($\pm$3.0)
		(2) 15.4 ($\pm$4.7)	(2) 7.9	(2) 0.5 ($\pm$0.4)	NZ $\leftrightarrow$ ND
K6A	H276E	(1) 2.8 ($\pm$1.2)	(1) 8.9	(1) $-$0.9 ($\pm$0.5)[a]	
		(2) 4.2 ($\pm$0.4)	(2) 8.7	(2) 0.5 ($\pm$0.4)[a]	
K6A	D280A	(1) n.d.	(1) <5.4	(1) —	14.8 ($\pm$3.3)
		(2) n.d.	(2) <5.4	(2) <$-$0.2 ($\pm$0.2)	NZ $\leftrightarrow$ OD
K7A	D275A	(1) n.d.	(1) <5.4	(1) —	12.0 ($\pm$1.9)
		(2) n.d.	(2) <5.4	(2) —	NZ $\leftrightarrow$ OD
K7A	H276A	(1) 89.7 ($\pm$18.5)	(1) 6.9	(1) —	14.2 ($\pm$1.2)
		(2) n.d.	(2) <5.4	(2) —	NZ $\leftrightarrow$ ND
K7A	H276E	(1) 36.4 ($\pm$11.7)	(1) 7.4	(1) $-$1.7 ($\pm$0.8)[a]	
		(2) n.d.	(2) <5.4	(2) —	
K7A	D280A	(1) n.d.	(1) <5.4	(1) —	11.9 ($\pm$1.1)
		(2) n.d.	(2) <5.4	(2) —	NZ $\leftrightarrow$ OD

[a]ΔG_i value calculated from the interaction between E276 residue and the mutated residues in the N-terminal.

The binding affinity assays were performed in (1) 54.5 mM MOPS pH 7.0, 0.5 mM EDTA, 1 mM DTT and (2) 25 mM MOPS pH 7.0, 5 mM MgCl$_2$, 1 mM DTT at 25°C. The ΔG values in the fourth column refer to the dissociation process.

In cases where one of the energetic components of the thermodynamic cycle could not be calculated (n.d.), an upper limit value of <5.4 kcal/mol was used.
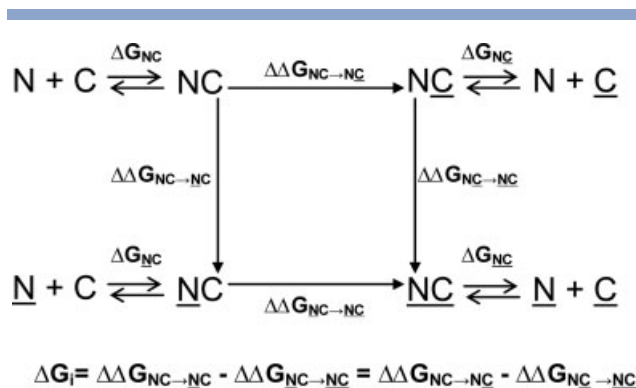
For some residue pairs, two or more energetic components of the thermodynamic cycle could not be calculated and therefore the coupling free energy could not be estimated (—).

The last column presents the average distance (above) between the indicated atoms (below) of the side-chains of the natural residues in the ensemble of solution structures of the head-to-tail complex.[14]

In columns 3 and 5, standard deviations from at least three replicated experiments are shown in parentheses.

of the free energies of association of wild-type (NC), single (N̲C, NC̲), and double-mutant fragments (N̲C̲) in a thermodynamic cycle (see Fig. 2). If the side chains of two residues N and C do not interact with one another, then the change in stability caused by one mutation in the wild-type complex ($\Delta\Delta G_{NC \rightarrow \underline{N}C}$ or $\Delta\Delta G_{NC \rightarrow N\underline{C}}$) will be the same as that observed for the same mutation in the presence of the second mutation ($\Delta\Delta G_{N\underline{C} \rightarrow \underline{N}\underline{C}} =$

Figure 2

Thermodynamic double-mutant cycle. The cycle is composed of the wild-type complex (NC), two single-mutant complexes (NC, NC), and a double-mutant complex (NC). From experimentally determined dissociation constants, it is possible to calculate the apparent free energy of head-to-tail complex formation (ΔG_{NC}) and the effects of each mutation ($\Delta\Delta G_{NC \to NC}$). The differences $\Delta\Delta G_{NC \to \underline{N}C}$ − $\Delta\Delta G_{N\underline{C} \to \underline{NC}}$ and $\Delta\Delta G_{NC \to N\underline{C}}$ − $\Delta\Delta G_{\underline{N}C \to \underline{NC}}$ lead to the free energy of coupling (ΔG_i) between the mutated residues. A positive ΔG_i value indicates a favorable interaction, while $\Delta G_i < 0$ a repulsive interaction between the side chains. When ΔG_i is equal to zero, the effects of mutating N and C are additive.

$\Delta\Delta G_{N\underline{C} \to \underline{NC}}$, $\Delta\Delta G_{NC \to N\underline{C}} = \Delta\Delta G_{\underline{N}C \to \underline{NC}}$). However, if the two side chains do interact, then the change in stability caused by the insertion of one mutation in the wild-type complex will be different from that caused by the same mutation in the presence of the second mutation ($\Delta\Delta G_{NC \to \underline{N}C} \neq \Delta\Delta G_{N\underline{C} \to \underline{NC}}$, $\Delta\Delta G_{NC \to N\underline{C}} \neq \Delta\Delta G_{\underline{N}C \to \underline{NC}}$). In this latter case, the resultant energy difference is the empirical free energy of coupling (ΔG_i) between the two mutated residues. A positive ΔG_i value indicates a favorable interaction: the double-mutant is less destabilized than what would be expected from the sum of the single-mutants' free energies of association. In the ideal case, the mutations affect only a specific interaction without significantly perturbing the remainder of the protein structure. Moreover, under favorable circumstances, solvation, electrostatic, and nonelectrostatic energies associated with structural changes caused by the mutations should cancel out in the cycle.[15–19]
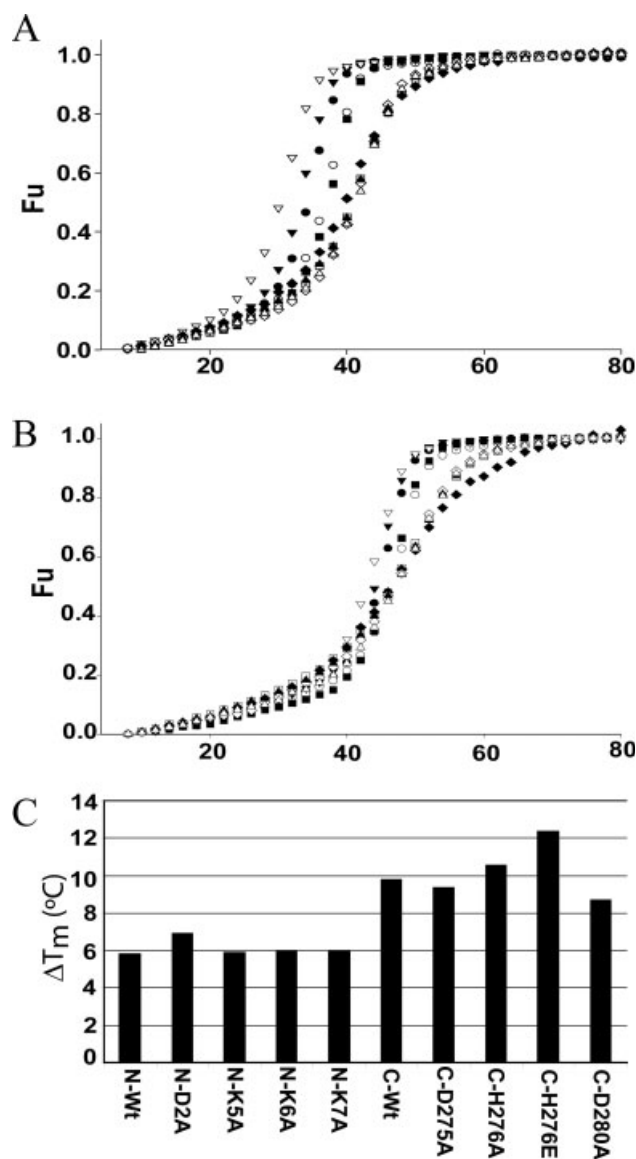
Apparent free energies of binding were calculated from the respective dissociation constants shown in Table II. Combinations of single and double-mutants were used in thermodynamic cycles to measure ΔG_i between residues with charged side chains (Table II). Using all combinations of the four N-terminal and C-terminal mutants under two conditions ($\pm Mg^{2+}$), thirty-two thermodynamic cycles were possible. However, as mentioned above, several single- or double-mutant complexes had affinities below the detection limit of the fluorescence assay. In these cases, a lower limit for K_d of the order of $1 \times 10^{-4} M$ was estimated, which allowed us to put an upper limit on the free energy of dissociation (5.4 kcal/

mol, Table II). If the cycle contained only one such imprecisely determined free energy of dissociation, then an upper or lower limit of the ΔG_i could be calculated. In this way, of the thirty-two possible thermodynamic cycles, twelve ΔG_i could be precisely calculated and a further five could be assigned upper or lower limit values. The remaining fifteen ΔG_i values could not be estimated at all (Table II). We note that the interaction energies were determined under conditions of low ionic strength ($I = 0.0254$), which is necessary to observe significant head-to-tail association at micromolar protein concentrations. On the other hand, the head-to-tail complex structure was determined at $I = 0.116$, which was possible due to the high protein concentrations ($\sim$1 mM).

An inspection of the data shown in Table II reveals that most of the pairwise interactions whose ΔG_i values could be estimated showed small interaction energies. Some of the residue pairs that displayed favorable ΔG_is in the presence of Mg^{2+} (D2–H276, 1.0 kcal/mol; K5–E276, 1.2 kcal/mol) showed unfavorable ΔG_is in the absence of Mg^{2+} (D2–H276, −0.9 kcal/mol; K5–E276, <−5.3 kcal/mol). The presence of Mg^{2+} also affected the interaction of H276 with K6. In the presence of this ion, the pairwise interactions did not present significant ΔG_i values (0.5 kcal/mol), but in the absence of Mg^{2+}, the interaction was unfavorable (K6–H276: −0.7 kcal/mol). Furthermore, the change of H276 to E276 did not result in favorable interactions with K5 and K6 in the absence of Mg^{2+} ($\Delta G_i < -0.9$ kcal/mol). Finally, the addition of Mg^{2+} ions converted some favorable interactions into unfavorable ones (K5–D280; K6–D280). Thus, Mg^{2+} seems to affect the coupling energy between charged residues in a complex manner, sometimes increasing and sometimes decreasing the interaction and in some cases converting favorable interactions to unfavorable ones (or vice-versa).

Thermal denaturations

The effect of the mutations on the stability of Tm fragments was analyzed by thermal denaturation accompanied by circular dichroism (see Fig. 3). In the absence of Mg^{2+}, all N-terminal fragments presented similar temperature denaturation profiles, with transition midpoint temperatures (T_m) close to 40°C. In the case of the C-terminal fragments, all mutations affected the stability compared to wild-type: D275A and D280A increased the stability ($\sim$+2.5°C), while H276A and H276E reduced the stability by 1.3 and 4.3°C, respectively. Addition of Mg^{2+} resulted in significant increases in the conformational energy of all the fragments. The addition of Mg^{2+} resulted in similar stability increases for all N-terminal fragments by $\sim$+6°C. In the case of the C-terminal fragment mutants, the relative stabilities between mutants were maintained; however, the stability gain upon addition of Mg^{2+} was dependent on the mutation. Mutants removing negatively charged side chains (D275A and D280A) had a reduced stability gain ($\sim$+9°C), com-

pared to H276A and H276E, which showed increases of 10.4 and 12.4°C, respectively [Fig. 3(C)].

Protein–protein docking

We used the protein docking program HADDOCK[28] to build a model of the structures of the head-to-tail complex formed by the polypeptide sequences, which we used in the double-mutant cycle analysis. To evaluate the docking methodology (see Methods section), we first calculated the head-to-tail complex starting from the original peptide structures of the NMR molecular model,[14] in combination with our mutagenesis data to drive the docking. Figure 4(A) shows that the resulting models are very similar to the NMR solution (the average backbone RMSD with respect to the best NMR model is 2.0 ± 0.2 Å). The main difference is that in most of the docking solutions, the N-terminal coiled-coil is slightly less inserted into the splayed helical chains of the C-terminal fragment [Fig. 4(A)]. Only a few contacts present in the NMR structure were not observed in the docking solutions: M1–L278, G(0)–A277, I4–L278, K5–A277, K5–M281 [Fig. 4(B,C)]. On the other hand, several new interactions were observed: M1–D280, M1–M281, A3–M281, K7–L278, K7–M281, M8–D280, M8–S283, M10–S283, M10–I284, D14–I284 [Fig. 4(B,C)]. The large number of experimental geometric restraints used in the NMR calculation allows a better definition of the interface than in the docking models. When the docking methodology was used to generate the wild-type complex used in our studies, the resultant model was also very similar to that of the NMR structure (RMSD 1.8 ± 0.2 Å) and highly similar to the docked NMR peptides (RMSD 0.7 ± 0.2 Å). Therefore, the difference between the NMR and docking solutions is not simply due to the Ala–Ser extension compared to the single Gly residue in the NMR structure, even though this extra amino acid could be expected to impede the penetration of the remaining N-terminal sequence into the cleft between the C-terminal chains. Nevertheless, the results demonstrated that the information (symmetry restraints and AIRs) we used to drive the docking is sufficient to generate a molecular model very similar to the one calculated using NMR data.[14] The intermolecular contacts (hydrogen bonds and hydrophobic interactions) observed in these models and the NMR structures are compared in Table III.

Our goal was to use docking to gain structural insight and rationalize the effects of the various mutations on the stability of the complex. We therefore carried out docking calculations with selected single and double-mutants (D2A, K6A, K7A, D275A, H276A, H276E, D2A–D275A, D2A–H276A, D2A–H276E, K6A–H276A, K6A–H276E, K7A–H276A, K7A–H276E). Complexes containing mutants K5A and D280A were not studied by docking, because these two residues were defined as active and used to drive the docking (see Methods section). Figure 5(A)
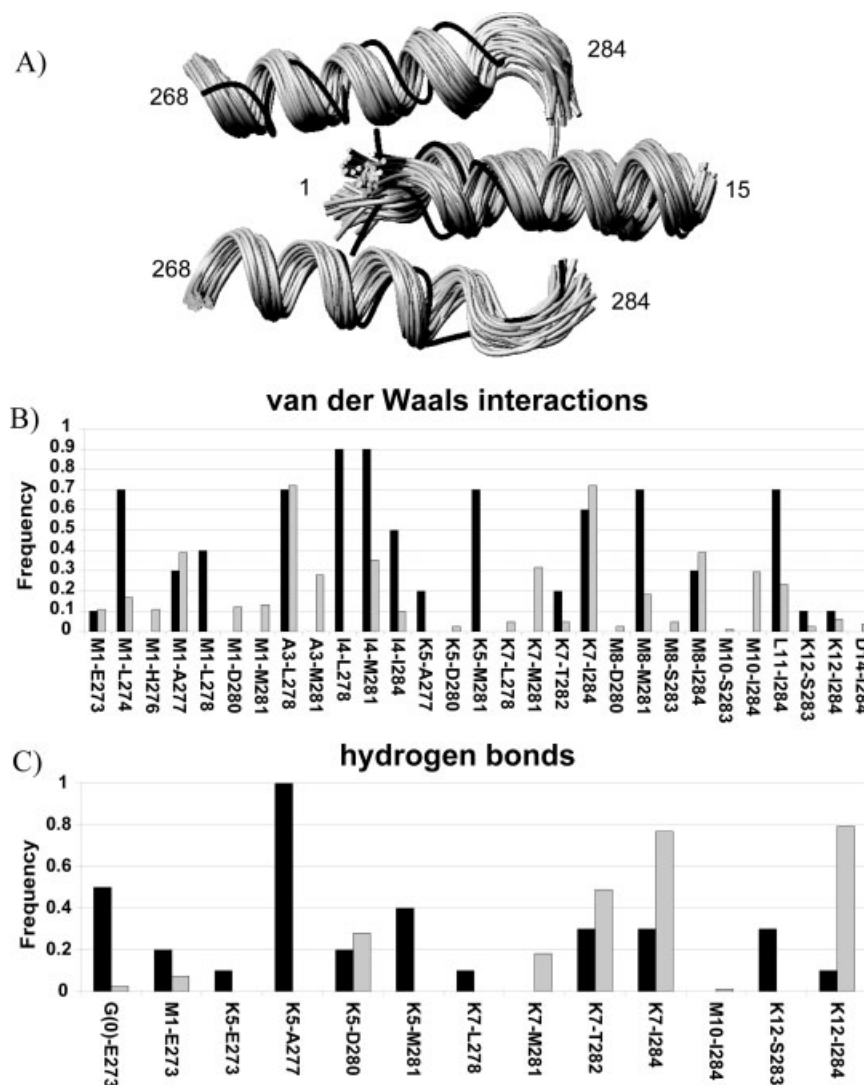

Figure 3

Thermal denaturation curves of ASTm$_{1–142}$, Tm$_{143–284(5OHW269)}$, and their mutants in the absence and presence of Mg^{2+}. The curves show the fraction of unfolded protein (Fu) determined by ellipticity at 222 nm as function of temperature (°C). (**A**) Denaturation profiles obtained in 54.5 mM MOPS pH 7.0, 0.5 mM EDTA, 1 mM DTT. (**B**) Denaturation profiles obtained in 25 mM MOPS pH 7.0, 5 mM MgCl$_2$ and 1 mM DTT. (**C**) Difference in the transition temperature (ΔT$_m$) observed in the presence and absence of 5 mM MgCl$_2$. Conditions in (**A**) and (**B**) have equivalent ionic strengths. In (**A**) and (**B**), symbols and denaturation transition temperatures in the absence and presence of Mg^{2+} are indicated for each fragment in that order: Tm$_{143–284(5OHW269)}$: ●, 34.1 and 43.9°C; Tm$_{143–284(5OHW269)}$D275A: ○, 36.4 and 45.8°C; Tm$_{143–284(5OHW269)}$ H276A: ▼, 32.7 and 43.3°C; Tm$_{143–284(5OHW269)}$H276E: ▽, 29.8 and 42.2°C; Tm$_{143–284(5OHW269)}$D280A: ■, 36.9 and 45.6°C; ASTm$_{1–142}$ A: □, 40.6 and 46.4°C; ASTm$_{1–142}$D2A: ◆, 39.5 and 46.4°C; ASTm$_{1–142}$K5A: ◇, 40.8 and 46.7°C; ASTm$_{1–142}$K6A: ▲, 40.6 and 46.6°C; ASTm$_{1–142}$K7A: △, 41.0 and 47.0°C.

Figure 4

Testing of the docking procedure using the NMR solution structure of the head-to-tail complex. (**A**) Docking solutions (gray) are compared with the most representative NMR structure (black). (**B**) Comparison of van der Waals contacts of NMR structures[14] (10 structures, 2G9J) with those observed in the docked models (63 structures). (**C**) Comparison of hydrogen bond contacts of NMR structures with docked models. In (B) and (C), black and gray bars represent the fraction of structures in which each specific contact was observed in the NMR and docking models, respectively. The contacts were identified using the program LIGPLOT.[33] The structures were drawn with MOLMOL.[35]

shows that while some mutants produced at least one cluster of docking solutions with relatively low RMSD (<2.5 Å) when compared to the wild-type model, the docking solutions for the D2A, H276A, and H276E single-mutant complexes and the D2A–H276E, K7A–H276A, and K7A–H276E double-mutant complexes all presented high RMSD values (>3.5 Å). Although these docking simulations were based on the same restraints, the principal feature that separated these two groups of models is that, in the high RMSD structures, the insertion of the N-terminal coiled-coil into the C-terminal cleft was significantly reduced. This is reflected in their low buried surface area (BSA) when compared to the models of low RMSD [Fig. 5(B)]. We chose to analyze the intermolecular contacts of the solutions in clusters, which presented lower RMSD deviation (<2.5 Å) with the wild-type model, since it is unlikely that those models with high RMSD values could be related to real molecular conformations. The number of structures (out of 200 calculated models in each simulation) in the cluster that converged most closely to the NMR structure varied for each mutant (from 5 for K7A to 146 structures for K6A–H276E, Table IV) as would be expected for residues involved in inter- or intramolecular contacts at the head-to-tail interface.

Table III
Intermolecular Hydrogen Bond and Hydrophobic Contacts Observed in the Docking Solutions for the Wild-Type Complex and Those Observed in the NMR Structures[14]
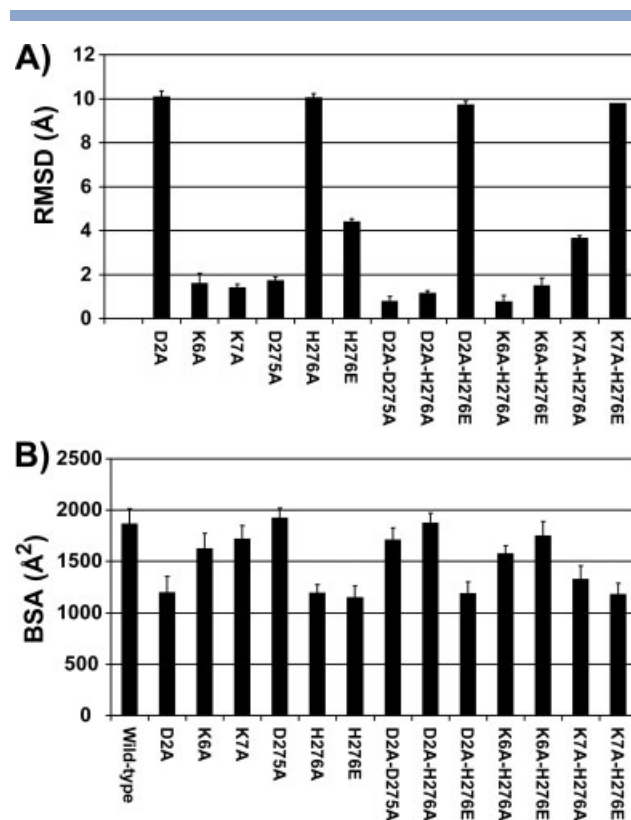
Hydrogen bonds		Van der Waals interactions		
A(−1)–E273 (b–s)	K7–A277 (s–b)	A(−1)–E273	*I4–L278*	M8–M281
G(0)–E273 (b–s)	K7–L278 (s–b)	*G(0)–E273*	I4–M281	M8–I284
M1–E273 (b–s)	K7–T282 (s–b)	*G(0)–A277*	*I4–I284*	M10–S283
K5–E273 (s–s)	K7–S283 (s–s)	M1–E273	*K5–A277*	M10–I284
K5–A277 (s–b)	K7–I284 (s–b)	M1–L274	K5–M281	L11–M281
K5–D280 (s–s)	*K12–S283* (s–s)	M1–H276	K7–L278	L11–I284
K5–M281 (s–b)	K12–I284 (s–b)	M1–A277	K7–M281	*K12–S283*
K7–M281 (s–b)		M1–L278	*K7–T282*	K12–I284
		A3–L278	K7–I284	D14–I284
		I4–A277	M8–D280	

The intermolecular hydrogen bonds and van der Waals interactions were identified using the program LIGPLOT.[33] Only contacts closer than 3.9 Å are listed; therefore, some interactions observed in the NMR structure up to 5 Å may not be listed. The contacts identified in the 23 docking solutions are in regular type and those identified in the 10 structures of the NMR ensemble[14] are in italic; those identified in both models are underlined. (s–s) indicates hydrogen bond contacts between side-chain atoms from both residues; (s–b) and (b–s) indicate hydrogen bond contacts between the side-chain of the first residue with a backbone group from the second residue or vice-versa.

We carried out an extensive comparison of the intermolecular hydrophobic and hydrogen bond contacts observed in the docked mutant complexes with the wild-type docking model and the NMR structure. Tables IV (hydrophobic contacts) and V (hydrogen bonds) show the fraction of docking models or NMR-derived models in which a specific interaction was observed. Many of the hydrophobic contacts between residues in "a" and "d" positions, which stabilize the head-to-tail interface,[14] were maintained in all docking solutions: M1(a)–L274(a), M1(a)–A277(d), I4(d)–A277(a), I4(d)–M281(a), M8(a)–I284(d), L11(d)–I284(d). The analysis also shows that residue K7 contributes significantly to the stability of the interface in the mutant models by participating in a large number of intermolecular contacts. This is consistent with the drastic reductions in head-to-tail complex stability observed for this mutant. The docking simulation of the K7A mutant generated only five models with low RMSD value to the NMR structure (1.42 ± 0.49 Å) (out of a total of 200). An analysis of these complexes show that not only the interactions formed by K7, but also the ones formed by neighboring residues, were disrupted (M8–281, M10–S283, L11–M281) (Tables IV and V).

While the K6A mutation did not affect the stability of the N-terminal fragment, it did reduce the stability of the head-to-tail complex. The docking model for mutant K6A in complex with the wild-type N-terminal does not present many significant structural changes in the head-to-tail interface in comparison to the wild-type model (Tables IV and V), and K6 does not participate in significant intermolecular contacts in the NMR solution structure, since it is pointing away from the interface (Tables IV

and V and Fig. 6; Ref. 14). However, as can be seen in Fig. 6(A), the replacement of Lys for Ala at this position disrupted the salt bridge interaction between D2 and K6 with the result that the carboxyl group from the D2 side chain is aligned differently in the mutant and wild-type models. The absence of the K6–D2 salt bridge could thus cause a local instability in the N-terminal interface, which disfavors complex formation. This effect is not observed in the case of the D2A mutant, possibly because K6 changes its orientation to interact with its neighbor Q9 [Fig. 6(B)]. The interaction of mutants H276A or H276E with K6A restored the binding affinity to values similar to the wild-type complex. Tables IV and V show that these double-mutants do not show significant differences in intermolecular contacts compared to the wild-type model. However, they do present additional interactions (D14–I284, K12–I284, L11–M281) when compared to the single-mutant K6A. These extra contacts could help to stabilize the head-to-tail interaction and in

Figure 5

Comparison of RMSD (Å) and buried surface area (BSA) among docking solutions for wild-type and mutant head-to-tail complexes. (**A**) RMSD of Cα, N, and C′ coordinates of the representative wild-type docking solution to the mutant complexes. (**B**) Buried surface area calculated by HADDOCK[28] for the wild-type and mutant complexes. Error bars correspond to the standard deviation of the RMSD and BSA values calculated from the best cluster of solutions from each docking simulation.

Table IV
Frequency of Appearance of van der Waals Contacts in the Wild-Type and Mutant-Docked Complexes

	Wild-type	PDB:2G9J	K6A	K7A	D275A	D2A D275A	D2A H276A	K6A H276A	K6A H276E
A(−1)–I270	—	—	—	—	0.04	—	—	—	—
A(−1)–E273	0.04	—	0.02	—	0.02	—	0.11	—	0.07
A(−1)–L274	—	—	—	—	—	—	0.01	—	—
S(0)–E273	—	—	—	—	0.55	—	—	—	0.14
S(0)–H276	—	—	—	—	0.09	—	—	—	—
M1–E273	0.26	0.10	0.28	0.20	0.34	0.17	0.27	0.18	0.21
M1–L274	0.09	0.70	0.04	—	0.60	0.07	0.14	0.01	0.17
M1–H276	0.09	—	0.13	—	0.38	0.03	—	—	—
M1–A277	0.52	0.30	0.51	0.80	0.43	0.58	0.81	0.69	0.71
M1–L278	0.04	0.40	0.04	0.20	—	—	0.04	0.03	—
M1–D280	—	—	0.11	—	—	0.01	—	0.01	0.02
M1–M281	—	—	0.04	0.20	0.02	0.01	0.02	0.01	—
A3–L278	0.96	0.70	0.47	1.00	0.43	0.92	0.81	0.95	0.48
A3–M281	—	—	0.04	0.20	0.09	0.01	—	—	0.02
I4–A277	0.39	—	0.19	0.20	0.17	0.43	0.33	—	0.12
I4–L278	—	0.90	—	—	—	—	—	0.01	—
I4–D280	—	—	—	—	—	—	0.02	—	0.10
I4–M281	0.48	0.90	0.83	0.60	0.32	0.61	0.42	—	0.74
I4–I284	—	0.50	0.06	0.20	—	0.01	0.03	—	0.02
K5–A277	—	0.20	—	—	—	—	—	—	—
K5–H276	—	—	—	—	0.06	—	—	—	—
K5–M281	—	0.70	—	—	—	—	—	—	—
K6–L278	—	—	—	—	—	0.01	0.19	—	—
K6–M281	—	—	—	0.20	—	—	0.06	—	—
K6–T282	—	—	—	—	—	0.01	0.01	—	—
K7–L278	0.09	—	0.04	—	—	0.15	0.06	0.29	—
K7–M281	0.52	—	0.60	—	0.68	0.33	0.43	0.75	0.52
K7–T282	—	0.20	—	—	—	—	—	—	0.02
K7–I284	0.09	0.60	0.38	—	0.70	0.13	0.06	0.01	0.24
M8–D280	0.09	—	—	—	0.02	0.03	—	0.01	—
M8–M281	0.48	0.70	0.17	—	0.34	0.19	0.47	0.27	0.31
M8–S283	—	—	—	—	0.02	—	—	—	—
M8–I284	0.30	0.30	0.04	0.40	0.15	0.11	0.16	0.15	0.19
M10–M281	—	—	—	—	—	0.18	0.09	0.14	0.05
M10–T282	—	—	0.02	—	—	0.31	0.44	0.05	0.05
M10–S283	0.13	—	0.11	—	0.02	0.42	0.50	0.17	0.62
M10–I284	0.52	—	0.21	0.40	0.47	0.32	0.50	0.25	0.71
L11–M281	0.04	—	—	—	—	0.21	0.01	0.16	0.02
L11–I284	0.52	0.70	0.13	0.40	0.23	0.40	0.37	0.34	0.14
K12–S283	—	0.10	—	—	—	—	—	—	—
K12–I284	0.04	0.10	—	—	0.04	0.06	—	0.08	—
D14–I284	0.09	—	—	—	—	0.38	0.15	0.04	0.12

Hydrophobic intermolecular contacts were analyzed using the LIGPLOT program.[33]
The frequency of appearance of a contact is the ratio of the number of structures where it is observed to the total number of structures.
Number of structures analyzed for each complex: wild-type (23 structures), K6A (47 structures), K7A (5 structures), D275A (47 structures), D2A–D275A (72 structures), D2A–H276A (117 structures), K6A–H276A (146 structures), K6A–H276E (42 structures); in the case of the NMR molecular model[14] (2G9J), all 10 deposited structures were analyzed.

this way compensate for the deleterious effects of the K6A mutation.

Even though the side chain of D275 points away from the complex interface, substitution of this residue for alanine greatly reduces binding to the N-terminal fragment. The docked structures of the D275A complex exhibit new intermolecular contacts in comparison to the wild-type model: A(−1)–I270, S(0)–E273, S(0)–H276, and K5–H276 (Tables IV and V). Figure 6(C) illustrates that the replacement of D275 for alanine resulted in the H276

side chain populating a different set of rotameric conformations, in which the imidazole group makes new contacts with residues in the N-terminal region [S(0), M1, and K5] (Tables IV and V). The proximity of the H276 side chain to the N-terminal α-NH$_3^+$ group and the K5 side chain could destabilize the head-to-tail complex, due to repulsive interactions. The H276 side chain is surrounded by several negatively charged residues: E272, E273, D275, and D280, and it could be expected that the conformation of the H276 side chain would be highly

Table V
Frequency of Appearance of Hydrogen Bonds in the Wild-Type and Mutant-Docked Complexes

	Wild-type	PDB:2G9J	K6A	K7A	D275A	D2A D275A	D2A H276A	K6A H276A	K6A H276E
A(−1)–E273	0.09	—	0.28	—	—	—	0.45	0.01	0.26
G(0)–E273	—	0.50	—	—	—	—	—	—	—
S(0)–E273	—	—	—	—	0.09	—	—	—	—
S(0)–H276	—	—	—	—	0.02	—	—	—	—
M1–E273	—	0.20	—	—	0.36	—	0.03	—	0.02
K5–E273	—	0.10	—	—	—	—	—	—	—
K5–A277	—	1.00	—	—	—	—	—	—	—
K5–D280	0.43	0.20	0.38	—	0.23	0.03	—	0.04	0.31
K5–M281	—	0.40	—	—	—	—	—	—	—
K6–M281	—	—	—	0.20	—	—	—	—	—
K6–T282	—	—	—	—	—	—	0.03	—	—
K6–I284	—	—	—	0.20	—	—	—	—	—
K7–A277	0.30	—	—	—	0.09	0.06	—	—	0.10
K7–L278	0.09	0.10	—	—	0.17	0.01	—	0.11	—
K7–D280	—	—	—	—	—	—	0.03	—	0.19
K7–M281	0.70	—	0.87	—	0.43	0.67	0.77	0.84	0.88
K7–T282	0.04	0.30	0.06	—	0.09	0.07	0.17	0.08	0.12
K7–S283	0.04	—	0.06	—	—	—	0.09	—	0.07
K7–I284	0.22	0.30	0.68	—	0.79	0.61	0.45	0.23	0.67
M10–I284	—	—	0.11	0.20	—	0.04	0.22	0.01	0.45
K12–S283	—	0.30	—	—	—	—	—	—	—
K12–I284	0.48	0.10	—	—	—	0.14	—	0.04	0.02

The structures were analyzed for hydrogen bonding intermolecular contacts using the LIGPLOT program.[33]
The frequency of appearance of a contact is the ratio of the number of structures where it is observed to the total number of structures.
The number of structures analyzed within each cluster are listed in Table IV.

sensitive to changes in charge density caused by mutating any one of these residues, including D275.
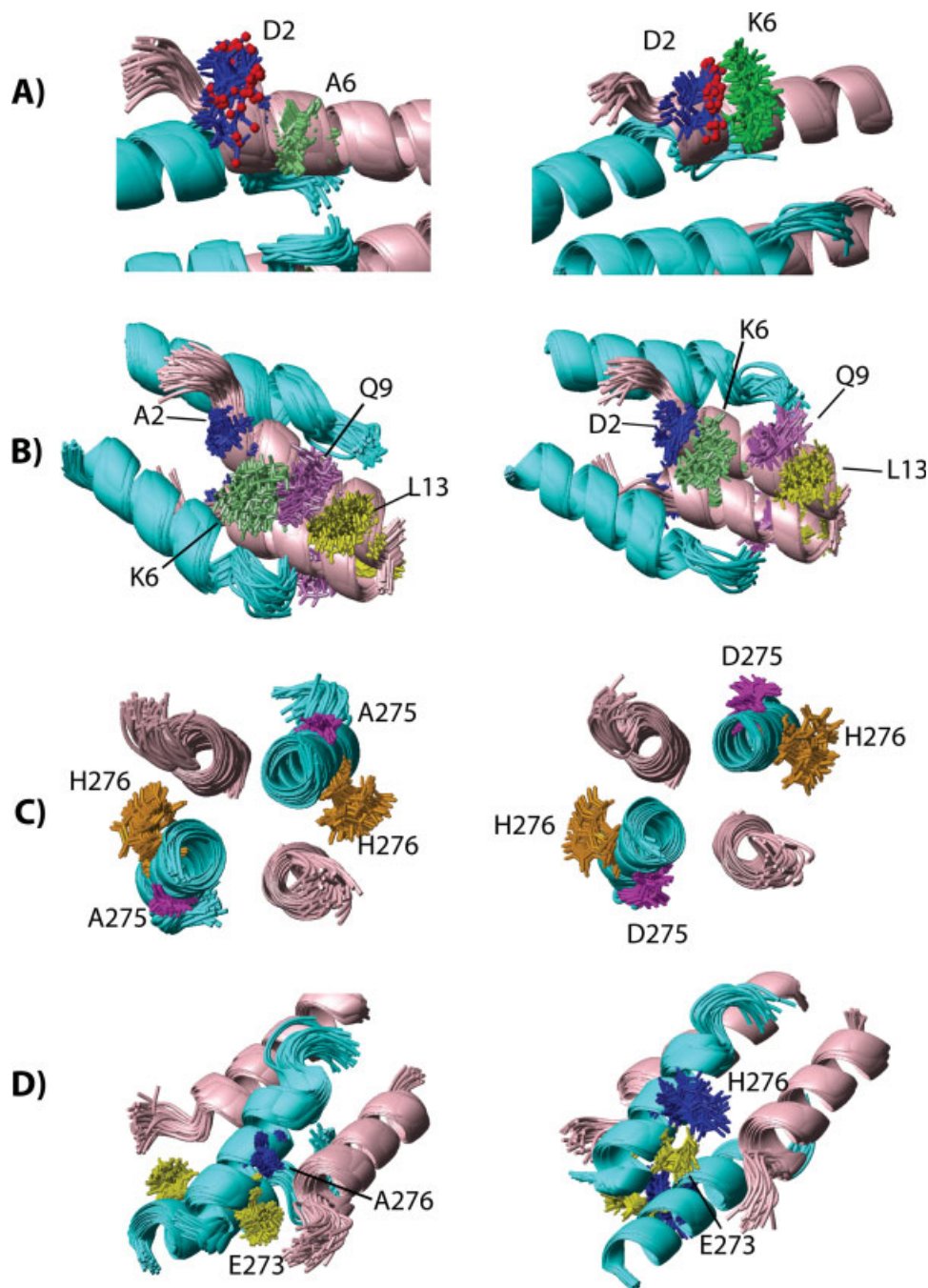
In the case of the double-mutant complex D2A–D275A, there are no observed contacts between His276 and residues in the N-terminal interface (Tables IV and V), which could explain the increase in affinity compared to the D275A single-mutant complex. Comparison of the docking models of the wild-type and D2A–D275A complexes [Fig. 6(B)] shows that the removal of the acidic side chain in D2 shifts the rotamer conformation of K6 away from A2 towards Q9. This in turn has the indirect effect of reducing intramolecular contacts between Q9 and L13 [Fig. 6(B)]. Furthermore, the D2A–D275A complex displays new contacts (Table IV): M10 forms more intermolecular interactions (M10–M281 and M10–T282) and there is a new contact involving residues D14 and I284 far from the N-terminal extremity.

The double-mutant D2A–H276A is more stable than the wild-type complex (K_d reduced from 4.4×10^{-7} M to 2.8×10^{-8} M, Table II). To evaluate the structural reasons for this change in complex stability we also performed a docking simulation of the D2A–H276A mutant complex. The H276 side chain interacts via a salt bridge with the E273 side chain in the NMR structure[14] and in a significant number of the wild-type docking structures [Fig. 6(D)]. Interestingly, the removal of the H276 side chain allowed the carboxyl side chain of residue E273 to interact with the α-NH$_3^+$ N-terminal extremity [A(−1)–

E273]. This has the effect of converting an intramolecular contact into an intermolecular one. Furthermore, the D2A mutation also allowed residue K6 to change its orientation and form intermolecular contacts with the C-terminal fragment (K6–L278, K6–M281, K6–T282) [Tables IV and V and Fig. 6(B)]. The observed changes in the number of intermolecular contacts could explain the 40-fold, 2-fold, and 150-fold increases in stability observed for the H276A, D2A, and D2A–H276A complexes, respectively.

DISCUSSION

The ionic strength dependence of Tm polymerization indicates a significant role for electrostatic interactions in stabilizing the head-to-tail complex.[10–13] However, the precise structural features that mediate this dependence are as yet unknown. For example, Tm helices are destabilized at low ionic strength, which at the same time stabilizes the head-to-tail complex.[22,23] The recently published NMR structure[14] showed that most of the intermolecular contacts in the complex interface are hydrophobic in nature, involving interactions among aliphatic side chains of "a" and "d" residues in the coiled-coil heptapeptide repeat. However, while the N-terminal fragment adopts a canonical coiled-coil conformation, the C-terminal fragment is not a coiled-coil in the NMR

Figure 6

Structural details of wild-type and mutant complexes. All figures show the ribbon diagrams of the C-terminal fragment in cyan and the N-terminal fragment in light pink. Stick models of specific residue side-chains are shown. (**A**) Comparison of K6A (left) and wild-type (right) complex docking models. The salt bridge formed by D2 and K6 in the wild-type model is lost in the K6A mutation, allowing the D2 side chain to adopt a different set of rotameric conformations. The hydroxyl groups from the D2 side chain are shown in red. (**B**) Comparison of D2A–D275A (left) and wild-type (right) complex docking models. The salt bridge formed by D2 and K6 in the wild-type model is lost upon D2A mutation. The K6 side chain therefore shifts in the direction of Q9, which consequently reduces the number of intramolecular contacts between Q9 and L13. (**C**) Comparison of D275A (left) and wild-type (right) complex docking models. The H276 side chain populates a different set of rotameric conformations in the two models. In the mutant structure, the H276 imidazole group approaches the N-terminal interface and make contacts with residues S(0), M1, and also K5 in some solutions (6% of the models). (**D**) Comparison of D2A–H276A (left) and wild-type (right) complex docking models. The loss of the E273–H276 salt-bridge in the mutant allows E273 to form intermolecular contacts with residues A(−1) and M1 in the N-terminal interface. All figures were produced with MOLMOL.[35]

structure.[14] Furthermore, there are contacts among residues in noncanonical coiled-coil positions: A3 (c) with L278 (e), K5 (e) with A277 (d) and M281 (a), and K7 (g) with M281 (a) and I284 (d). On the other hand, most of the ionic interactions in the overlap region were found to be intrachain (i, i + 3) and (i, i + 4). The few intermolecular electrostatic contacts, which were observed, involve the side chains of K5, K7, and K12 with the carboxyl group of I284, and the side chain amino group of K5 with the carboxyl side chain of D280 and E273. Despite the fact that a larger number of hydrophobic rather than electrostatic contacts were observed in the interface, the results described in the present study show that intra- and intermolecular ionic contacts made by K5, K7, and D280 are essential for the stability of the complex. Moreover, other charged residues (K6, D275, and H276) were also shown to be important for head-to-tail complex formation.

In the N-terminal region, the K5A and K7A mutations drastically reduced the stability of complex formation (Table II). These effects agree with the observations of Johnson and Smillie[6] who demonstrated that acetylation of K7 abolished Tm polymerization. In the NMR structure, this residue participates in hydrogen bonds and hydrophobic contacts with several C-terminal amino acids (M281, T282, S283, and I284) (Table III). In addition, the NMR structure also showed that K5 forms a salt bridge with D280 and makes hydrophobic contacts with A277 and M281.[14] On the other hand, while K6 is not part of the N-terminal binding surface,[14] mutating it to Ala reduces the binding affinity (Table II). In the C-terminal region, mutations of D275 or D280 to Ala severely reduced complex stability (Table II). In the latter case this is expected, since D280 was observed to form a salt-bridge with K5 (Ref. 14). However, D275 is completely exposed to the solvent and it is not involved in any intermolecular contact in the NMR structure.[14] Finally, mutations of H276 to Ala or Glu increased the affinity of the termini, even though H276 is also exposed to the solvent and does not participate in any intermolecular contacts in the NMR structure.[14]

We used protein–protein docking to try to rationalize the effect of some of the mutations on the interface in terms of structural contacts. In the case of the K7A single-mutant complex, in addition to the direct loss of several directly K7-dependent hydrogen bonds with C-terminal residues, other intermolecular contacts (M8–M281, M10–S283, L11–M281) were indirectly affected (Tables IV and V). As we used K5 and D280 as active residues to drive the docking of the termini, we did not calculate models for these mutants. However, as can be seen in NMR and docked wild-type structures, these residues form many hydrogen bonds and van der Waals contacts, which contribute to stabilize the interface. Some docking models (K6A, D275A, and D2A–D275A) show that some mutations not only affect intermolecular contacts, but also intramolecular ones. This helps us to rationalize how solvent-exposed residues such as K6A and D275A, which do not participate in direct intermolecular contacts in the complex interface, can contribute indirectly to complex stability. Docking structures of K6A-wild type and D2A–D275A showed that the D2A and K6A mutations changed the intramolecular contacts pattern in the N-terminal helix. The salt bridge between D2 and K6 side chains, which possibly contributes to stabilize the N-terminal extremity, was disrupted upon K6 substitution [Fig. 6(A)]; the local instability generated by this mutation could have an indirect and negative effect on complex formation. In the same way, the D2A mutation affects the interactions involving K6, Q9, and L13 side chains within the N-terminal helix [Fig. 6(B)]. Changes in the orientations of these side chains induced by the D2A mutation might explain the restoration of complex formation by the D275A mutant.

Thermal denaturations (see Fig. 3) of the C-terminal fragments showed that both mutations D275A and D280A caused an increase in the stability of the C-terminal fragments ($\sim+2°C$). This could be related to the lower helical propensity of aspartic acid compared to alanine.[36] Another factor, which could contribute to these differences in stability, is the fact that D275 and D280 are both localized in a region of high negative charge density (E272, E273, D275, D280, I284–COO$^-$). Repulsive interactions of D275 with E272 and E273 and of D280 with the carboxy-terminus would be relieved by these mutations. It is important to mention that, in this study, we used fragments containing the wild-type Asn residue at position 279 instead of the stabilizing Lys residue used in the NMR studies.[14,37] The K279 mutation increases the stability of the peptide, because it forms a salt-bridge interaction with D275 (Refs. 37–39). In the wild-type peptide, there is no stabilizing salt-bridge interaction.

The H276A and H276E mutations reduced the stability of the C-terminal fragment. Substitution of H276 by Ala or Glu possibly affects the stability of this region, because the mutants can no longer form intramolecular salt bridge interactions with E272, E273, and D280 as observed in the NMR structure.[14] Furthermore, addition of a Glu residue causes an increase in the number of negatively charged residues, elevating the number of repulsive interactions, therefore destabilizing the fragment.

The intrinsic flexibility in the C-terminal region appears to be essential for head-to-tail formation.[14,37–40] We previously showed that buffer conditions, which increase the stability of Tm fragments, have an opposite effect on the stability of the complex.[22,23] The NMR structure clearly demonstrated that the C-terminal region must be flexible enough to break interhelical contacts to allow the insertion of the N-terminal coiled-coil dimer.[14] We note that for all four C-terminal mutants tested, those that increased conformational stability resulted in reduced stability of the head-to-tail complex (no such

correlation was observed for the N-terminal fragment mutants). Thus, the effects of the mutations on the affinities might not simply be a result of the deletion of interactions between residues, but also from changes in coiled-coil stability and flexibility.

The effects of Mg^{2+} on the binding affinities indicate that this ion possibly affects the orientation and interaction of the side-chains in the head-to-tail interface. Thermal denaturations clearly showed that this ion has a significant effect on the stability of the isolated fragments. C-terminal fragments are especially stabilized by Mg^{2+}, presenting increases in thermal stability of ~10°C (see Fig. 3). It is also important to note that the increments in the stability in this region were dependent on the mutation [Fig. 3(C)]: while the H276E mutant destabilized the fragment significantly in the absence of Mg^{2+}, the addition of this divalent cation restores stability to near wild-type values. Thus, the Mg^{2+}-induced increment in stability for this fragment was 2.6°C greater than that of the wild-type fragment. These observations indicate that Mg^{2+} apparently binds to the C-terminal fragment in the head-to-tail complex.

The C-terminal region is rich in acidic residues (S**EEL**D**HALN**D**MTSI), which could act as sites for Mg^{2+} binding and could mediate salt bridge interactions among the negatively charged side chains of residues E272, E273, D275, D280, and I284 (COO^-). These intramolecular Mg^{2+}-mediated salt bridges could, however, affect intermolecular head-to-tail contacts in a complex manner. In fact, the affinities of the wild-type complex are highly similar in the absence and presence of Mg^{2+} (Table II). However, this cation did have significant influence on stability when specific residues were mutated. In specific cases, Mg^{2+} could be mediating intermolecular interactions between negatively charged residues in the interface. D2 is the only acidic residue of the N-terminal in the overlapping region. Mg^{2+} could allow the formation of salt bridges between this aminoacid with D280 and/or D275 or with backbone carbonyl oxygens of the C-terminal. The average distance between the oxygen atoms from the carboxyl groups of D2 and D275 or D280 is about 12 Å in the NMR structure that was determined in the absence of Mg^{2+} (Ref. 14). However, the addition of Mg^{2+} could favor the approach of these side chains and the formation of a salt bridge, consistent with the coupling free energy observed for the D2:D280 interaction (0.7 kcal/mol) in the presence of Mg^{2+} (Table II). However, we have to consider that, in the presence of Mg^{2+}, binding affinities measured for D280A and the double-mutant D2A–D280A also increased (Table II). Similarly, small but favorable ΔG_i (0.5 kcal/mol) observed for D2:E276 in the presence of Mg^{2+} vanished upon addition of EDTA. At this stage, we can deduce that Mg^{2+} binds to Tm and causes complex changes to the structures of termini and is possibly mediating additional interactions in the interface (also see below).

Coupling free energies are actually the sum of several energetic components[17]:

$$\Delta G_i = \Delta G_{N/solv} + \Delta G_{C/solv} + \Delta G_{T/NElect} + \Delta G_{T/CElect}$$
$$+ \Delta G_{T/Nnonelect} + \Delta G_{T/Cnonelect} + \Delta G_{reorg(N\,or\,C)}$$
$$- \Delta G'_{reorg(N\,or\,C)} - G_{NC} \quad (4)$$

where $\Delta G_{N/solv}$ and $\Delta G_{C/solv}$ are the changes in solvation energy of residue N due to a mutation of residue C and vice versa; $\Delta G_{T/NElect}$ and $\Delta G_{T/CElect}$ are the changes in the electrostatic energy upon mutating residues N or C in the wild-type complex; $\Delta G_{T/Nnonelect}$ and $\Delta G_{T/Cnonelect}$ are the changes in nonelectrostatic energy due to a mutation of N and C in the wild-type complex; $\Delta G_{reorg(N\,or\,C)} - \Delta G'_{reorg(N\,or\,C)}$ is the energy difference related to the structural reorganization caused by a mutation in the wild-type in respect to the same mutation in the single-mutant; and G_{NC} is the coulombic interaction energy between the pair of residues in the N- and C-terminal.

In the system under study, all of the mutated residues are exposed to solvent and of these, only residues K5 and D280 form an intermolecular (N–C terminal) ion pair in the NMR structure.[14] We therefore do not expect significant changes in solvation energy ($\Delta G_{N/solv} + \Delta G_{C/solv}$) upon mutation. As described above, the mutations introduced in the C-terminal region affected the stability of the isolated fragments, while the N-terminal fragments all presented similar stabilities (see Fig. 3). Therefore, considering that these stability differences may be due to modified electrostatic and nonelectrostatic energies, we cannot ignore the terms $\Delta G_{T/CElect} + \Delta G_{T/Cnonelect}$ from the ΔG_i calculation. Finally, due to the possible structural modifications caused by the mutations (as observed in the thermodynamic stability assays and the docking solutions), we cannot neglect the $\Delta G_{reorg(N\,or\,C)} - \Delta G'_{reorg(N\,or\,C)}$ energy term. Consequently, Eq. (4) could possibly be reduced to

$$\Delta G_i = \Delta G_{T/CElect} + \Delta G_{T/Cnonelect}$$
$$+ (\Delta G_{reorg(N\,or\,C)} - \Delta G'_{reorg(N\,or\,C)}) - G_{NC} \quad (5)$$

This leads to the conclusion that the observed interaction energy is actually composed of the summation of several energy terms such as coulombic interaction between the N and C residues, electrostatic, nonelectrostatic, and conformational energy terms. This might explain the measurement of unexpected interaction energies for residues observed to be distant in the NMR structure (D2–H276 ΔG_i: −0.9 kcal/mol, distance 17.4 Å; K6–D275 ΔG_i: < −0.3 kcal/mol, distance 16.1 Å), unfavorable ΔG_i values for interactions between opposite charged residues (K5–E276 ΔG_i < −5.3 kcal/mol; K5–D280 ΔG_i < −1.1 kcal/mol), and favorable ΔG_i for residue pairs of the same electrical charge (D2–D280 ΔG_i > 2.1 kcal/mol, in the absence of Mg^{2+}) (Table II).

The possibility exists that the most important intermolecular electrostatic interactions are in fact between residues for which the coupling energy could not be determined, since the mutation of one or more of these residues could be expected to reduce the stability of the complex so much that it could not be measured. Furthermore, the only short-distance intermolecular salt bridges observed between charged side chains in a small fraction of the NMR structure ensemble[14] were between residue K5 and residues D280 and E273 (Table III). In the absence of Mg^{2+}, either K5 or D280 mutations on their own reduce the head-to-tail interaction below the detection limit, consistent with a structural role for these residues in the stabilization of the complex (mutations at position 273 were not studied). Unexpectedly, the measured coupling energy between K5 and D280 in the presence of Mg^{2+} was found to be slightly unfavorable (< -1.1 kcal/mol, Table II). This repulsive effect could be explained, however, if Mg^{2+} binds specifically to D280, effectively converting its net charge from -1 to $+1$. The binding of cations to negatively charged residues has been shown to disrupt interhelical ion pairs in coiled-coils.[41]

Most of the calculated pairwise interactions had small ΔG_i values and involved pairs of residues distant from one another in the docked structures (Table II). Small ΔG_i values have been observed for noncontacting charged residues in staphylococcal nuclease,[42] idiotope-antiidiotope complex,[43] and the barnase–barstar complex.[44] Goldman et al.[43] proposed that the energy of interaction for distant residues may result from the effects on the protein conformation and/or solvent rearrangements in the protein–protein interface, which may result in long-range perturbations in electrostatic fields within the interface. Furthermore, solvent-exposed ion pairs have smaller energies of interaction in comparison to buried electrostatic interactions.[18,43–47] This can be explained by several factors: (i) the higher dielectric constant at the protein surface when compared to the protein core (the enthalpy of interaction between two buried charges should be larger than that between two solvent-exposed charges[47,48]); (ii) the entropy cost involved in the formation of a salt bridge at the surface, because two freely rotating groups of opposite charge must be held in a restricted position[45,47]; and (iii) the high desolvation energy cost involved in the formation of salt bridges.[49]

[15]N relaxation data detected significant overall backbone flexibility in the Tm junction interface as well as conformational variability at specific positions.[14] This variability could be of physiological significance by permitting the head-to-tail complex to adopt a number of conformational states that could be differentially populated in the different regulatory states of the thin filament (blocked, closed, and open).[14] The large number of small coupling energies for specific pairs of charged residues in the head-to-tail interface and their complex sensitivities to the presence of Mg^{2+} are consistent with the above

hypothesis as are the results of our docking simulations that showed that the pattern of ionic contacts throughout the interface was highly sensitive to the presence or absence of specific contacts.

REFERENCES

1. Farah CS, Reinach FC. The troponin complex and regulation of muscle contraction. FASEB J 1995;9:755–767.
2. Gordon AM, Homsher E, Regnier M. Regulation of contraction in striated muscle. Physiol Rev 2000;80:853–924.
3. McLachlan AD, Stewart M. Tropomyosin coiled-coil interactions: evidence for an unstaggered structure. J Mol Biol 1975;98:293–304.
4. McLachlan AD, Stewart M. The 14-fold periodicity in alpha-tropomyosin and the interaction with actin. J Mol Biol 1976;103:271–298.
5. Cohen C, Caspar DL, Parry DA, Lucas RM. Tropomyosin crystal dynamics. Cold Spring Harb Symp Quant Biol 1972;36:205–216.
6. Johnson P, Smillie LB. Polymerizability of rabbit skeletal tropomyosin: effects of enzymatic and chemical modifications. Biochemistry 1977;16:2264–2269.
7. Mak A, Smillie LB, Barany M. Specific phosphorilation at serine-283 of alpha tropomyosin from frog skeletal and rabbit skeletal cardiac muscle. Proc Natl Acad Sci USA 1978;75:3588–3592.
8. Heeley DH, Watson MH, Mak AS, Dubord P, Smillie LB. Effect of phosphorilation on the interaction and functional properties of rabbit striated muscle αα-tropomyosin. J Biol Chem 1989;264:2424–2430.
9. Sano KI, Maeda K, Oda T, Maeda Y. The effect of single residue substitutions of Serine-283 on the strength of the head-to-tail interaction and actin binding properties of rabbit skeletal muscle α-tropomyosin. J Biochem 2000;127:1095–1102.
10. Tsao TC, Bailey K, Adair GS. The size shape and aggregation of tropomyosin particles. Biochem J 1951;49:27–36.
11. Kay CM, Bailey K. Light scattering in solutions of native and guanidinated rabbit tropomyosin. Biochim Biophys Acta 1960;40:149–156.
12. McCubbin WD, Kay CM. Physicochemical studies on the aggregation of bovine cardiac tropomyosin with ionic strength. Can J Biochem 1969;47:411–414.
13. Sousa AD, Farah CS. Quantitative analysis of tropomyosin linear polymerization equilibrium as a function of ionic strength. J Biol Chem 2002;277:2081–2088.
14. Greenfield NJ, Huang YJ, Swapna GVT, Bhattacharaya A, Rapp B, Singh A, Montelione GT, Hitchcock-DeGregori SE. Solution NMR structure of the junction between tropomyosin molecules: implications for actin binding and regulation. J Mol Biol 2006;364:80–96.
15. Carter PJ, Winter G, Wilkinson AJ, Fersht AR. The use of double mutants do detect structural changes in the active site of the tyrosil-tRNA synthetase (Bacillus stearothermophilus). Cell 1984;38:835–840.
16. Horovitz A, Serrano L, Avron B, Bycroft M, Fersht AR. Strenght and co-operativity of contributions of surface salt bridges to protein stability. J Mol Biol 1990;216:1031–1044.
17. Serrano L, Horovitz A, Avron B, Bycroft M, Fersht AR. Estimating the contribution of engineered surface electrostatic interactions to protein stability by using double-mutant cycles. Biochemistry 1990;29:9343–9352.
18. Horovitz A. Double-mutant cycles: a powerful tool for analyzing protein structure and function. Fold Des 1996;1:121–126.
19. Bosshard HR, Marti DN, Jelesarov I. Protein stabilization by salt bridges: concepts experimental approaches and clarification of some misunderstandings. J Mol Recognit 2004;17:1–16.
20. Monteiro PB, Lataro RC, Ferro AJ, Reinach FC. Functional alpha-tropomyosin produced in Escherichia coli. A dipeptide extension

can substitute the amino-terminal acetyl group. J Biol Chem 1994;269:10461–10466.

21. Farah CS, Reinach FC. Regulatory properties of recombinant tropomyosins containing 5-hydroxytryptophan: Ca^{2+} binding to troponin results in a conformational change in a region of tropomyosin outside the troponin binding site. Biochemistry 1999;38:10543–10551.

22. Paulucci AA, Katsuyama AM, Sousa AD, Farah CS. A specific C-terminal deletion in tropomyosin results in a stronger head-to-tail interaction and increased polymerization. Eur J Biochem 2004;271:589–600.

23. Corrêa F, Farah CS. Different effects of trifluoroethanol and glycerol on the stability of tropomyosin helices and the head-to-tail complex. Biophys J 2007;92:2463–2475.

24. Hartree EF. Determination of protein: a modification of the Lowry method that gives a linear photometric response. Anal Biochem 1972;48:422–427.

25. Wandschneider E, Hammack BN, Bowler BE. Evaluation of cooperative interactions between substructures of iso-1-cytochrome c using double mutant cycles. Biochemistry 2003;42:10659–10666.

26. Sali A, Blundell TL. Comparative protein modeling by satisfaction of spatial restrains. J Mol Biol 1993;234:779–815.

27. Brunger AT, Adams PD, Clore GM, Delano WL, Gros P, Grosse-Kunstleve RW, Jiang JS, Kuszewski J, Nilges M, Pannu NS, Read RJ, Rice LM, Simonson T, Warren GL. Crystallography & NMR system: a new software suite for macromolecular structure determination. Acta Crystallogr D Biol Crystallogr 1998;54:905–921.

28. Dominguez C, Boelens R, Bonvin AMJJ. HADDOCK: a protein–protein docking approach based on biochemical and/or biophysical information. J Am Chem Soc 2003;125:1731–1737.

29. Linge JP, Williams MA, Spronk CA, Bonvin AMJJ, Nilges M. Refinement of protein structures in explicit solvent. Proteins 2003;50:496–506.

30. van Dijck M, van Dijck ADJ, Hsu V, Boelens R, Bonvin AMJJ. Information-driven protein-DNA docking using HADDOCK: it is a matter of flexibility. Nucleic Acids Res 2006;34:3317–3325.

31. Nilges M, Brünger AT. Automated modeling of coiled coils: application to the GCN4 dimerization region. Protein Eng 1991;4:649–659.

32. Nilges M. A calculation strategy for the structure determination of symmetric dimers by ^{1}H NMR. Proteins 1993;17:297–309.

33. Wallace AC, Laskowski RA, Thornton JM. LIGPLOT: a program to generate schematic diagrams of protein–ligand interactions. Protein Eng 1995;8:127–134.

34. Corrêa F, Farah CS. Using 5-hydroxytryptophan as a probe to follow protein-protein interactions and protein folding transitions. Protein Pept Lett 2005;12:241–244.

35. Koradi R, Billeter M, Wutrich K. MOLMOL: a program for display and analysis of macromolecular structures. J Mol Graph 1996;14:29–32,51–55.

36. Chou PY, Fasman GD. Empirical predictions of protein conformation. Annu Rev Biochem 1978;47:251–276.

37. Palm T, Grabosky S, Hitchcock-DeGregori SE, Greenfield NJ. Disease-causing mutations in cardiac troponin T: identification of a critical tropomyosin-binding region. Biophys J 2001;81:2827–2837.

38. Greenfield NJ, Palm T, Hitchcock-DeGregori SE. Structure and interactions of the carboxyl terminus of striated muscle α-tropomyosin: it is important to be flexible. Biophys J 2002;83:2754–2766.

39. Greenfield NJ, Swapna GVT, Huang Y, Palm T, Graboski S, Montelione GT, Hitchcock-DeGregori SE. The structure of the carboxyl terminus of striated α-tropomyosin in solution reveals an unusual parallel arrangement of interacting α-helices. Biochemistry 2003;42:614–619.

40. Li Y, Mui S, Brown JH, Strand J, Reshetnikova L, Tobacman LS, Cohen C. The crystal structure of the C-terminal fragment of striated-muscle α-tropomyosin reveals a key troponin T recognition site. Proc Natl Acad Sci USA 2002;28:7378–7383.

41. Kohn WD, Kay CM, Hodges RS. Salt effects on protein stability: two stranded α-helical coiled-coils containing inter- or intrahelical ion pairs. J Mol Biol 1997;267:1039–1052.

42. Green MS, Shortle D. Patterns of nonadditivity between pairs of stability mutations in Staphylococcal nuclease. Biochemistry 1993;32:10131–10139.

43. Goldman ER, Dall'Acqua W, Braden BC, Mariuzza RA. Analysis of binding interactions in an idiotope–antiidiotope protein–protein complex by double mutant cycles. Biochemistry 1997;36:49–56.

44. Schreiber G, Fersht AR. Energetics of protein–protein interactions: analysis of the barnase–barstar interface by single mutations and double mutant cycles. J Mol Biol 1995;248:478–486.

45. Dao-pin S, Sauer U, Nicholson H, Matthews BW. Contributions of engineered surface salt bridges to the stability of T4 lysozyme determined by directed mutagenesis. Biochemistry 1991;30:7142–7153.

46. de Prat-Gay G, Johnson CM, Fersht AR. Contribution of a proline residue and a salt bridge to the stability of a type I reverse turn in chymotrypsin inhibitor-2. Protein Eng 1994;7:103–8.

47. Sali D, Bycroft M, Fersht AR. Surface electrostatic interactions contribute little of stability of barnase. J Mol Biol 1991;220:779–788.

48. Warshel A, Russel ST. Calculations of electrostatic interactions in biological systems and in solutions. Quart Rev Biophys 1984;17:283–422.

49. Hendsch ZS, Tidor B. Do salt bridges stabilize proteins? A continuum electrostatic analysis. Protein Sci 1994;3:211–226.